Li+ ion doping: an approach for improving the crystallinity and upconversion emissions of NaYF4:Yb3+, Tm3+ nanoparticles

Zhao, C.; Kong, X.; Liu, X.; Tu, L.; Wu, F.; Zhang, Y.; Liu, K.; Zeng, Q.; Zhang, H.

DOI
10.1039/c3nr01916k

Publication date
2013

Document Version
Final published version

Published in
Nanoscale

Nanoscale

RSC Publishing

PAPER

View Article Online
View Journal | View Issue

Cite this: *Nanoscale*, 2013, **5**, 8084

Li^+ ion doping: an approach for improving the crystallinity and upconversion emissions of $NaYF_4:Yb^{3+}$, Tm^{3+} nanoparticles†

Chengzhou Zhao,[ab] Xianggui Kong,*[a] Xiaomin Liu,[a] Langping Tu,[ab] Fei Wu,[ab] Youlin Zhang,[a] Kai Liu,[abc] Qinghui Zeng[a] and Hong Zhang*[c]

Received 17th April 2013
Accepted 31st May 2013

DOI: 10.1039/c3nr01916k

www.rsc.org/nanoscale

The application of upconversion nanoparticles (UCNPs), especially *in vivo*, has so far been hampered by their relatively low upconversion efficiency. In this work, a strategy of Li^+ doping was revisited with the aim of enhancing UV to blue UC luminescence of $NaYF_4:Yb^{3+}$, Tm^{3+} nanocrystals. We have demonstrated that the short wavelength UC emission bands were indeed significantly enhanced. Compared to lithium-free $NaYF_4:Yb^{3+}$, Tm^{3+}, the UC emission intensities of 452 nm and 479 nm of the NPs co-doped with 7 mol% Li^+ ions were increased by 8 and 5 times, respectively. The mechanism of the enhancement was discussed and the improvement of the nanoparticles' crystallinity and the distortion of the local symmetry around the Tm^{3+} ions, when the Li^+ ions were introduced, were confirmed to be the origin of the improvement.

1 Introduction

In recent years, upconversion (UC) luminescence of lanthanide-doped nanocrystals, especially inherent low phonon energy $NaYF_4$-based systems, has drawn considerable attention due to their unique optical properties and potential applications in fields such as volumetric displays,[1] temperature sensors,[2] UC lasers,[3] biomedical imaging,[4] DNA detection,[5] and photodynamic therapy.[8] However, the applications of these UC nanocrystals are still constrained because of their low UC efficiency. Various attempts have been devoted to improving this aspect, including both internal adjustments and external approaches, such as varying the crystal phase of the nanoparticles,[9] introducing a co-dopant sensitizer,[10] crystal surface coating,[11] the application of a core–shell structure,[12] and others.[13] Despite these efforts, which provide vast promise for its applications,[14] challenges are even more when short wavelength upconversion emission is required, where more than two photons are needed to generate a UC photon.

It is well established that the upconversion emission of rare-earth ion-doped materials is dependent on their intra 4f transition probabilities, which is significantly affected by the local crystal field symmetry of the rare-earth ions[15] and crystalline perfection. Due to its small ionic radius, Li^+ ions can be doped easily into the host lattice substitutionally or interstitially, which will break the symmetry of the crystal field around it, leading to the enhancement of the UC luminescence of Er^{3+} ion-doped nanocrystals.[16] For example Zhang's group reported significant enhancement of the visible UC radiation in $Y_2O_3:Yb^{3+}$, Er^{3+} nanocrystals by co-doping with Li^+ ions.[17] Cai *et al.* reported more than a 30-fold increase in $NaGdF_4:Yb^{3+}$, Er^{3+}.[18] Despite all this work, the underlying mechanism is not completely distinct. On the other hand, the electronic structure of Tm^{3+} is suitable for generating some specific upconversion emissions which are of significance for activating certain chemical or biological processes. For example, the violet UC light can be used to excite channelrhodopsins, which are a subfamily of opsin proteins that function as light-gated ion channels in neural cells, and to photochemical catalysis; blue UC nanocrystals are vital to realize multicolor fluorescence biolabels.[6,7] Blue UC emissions can also excite several FDA approved photosensitizers making it possible for use in cancer diagnosis and UC photodynamic therapy.[8] However, in the $NaYF_4$ host lattice, the violet and blue UC lights are too weak to use because the UC processes involve three or four photons.

To face the challenge, $NaYF_4:Yb^{3+}$, Tm^{3+} nanocrystals doped with Li^+ ions of various concentrations were studied in detail in this work. Significant UC luminescence enhancement was observed compared with their Li^+-free counterpart. Most importantly, the role of Li^+ in the UC enhancement was determined to be a joint effect of the perfection in the crystallinity and the distortion of the local symmetry of the emitters.

[a]*State Key Laboratory of Luminescence and Applications, Changchun Institute of Optics, Fine Mechanics and Physics, Chinese Academy of Sciences, Changchun 130033, China. E-mail: xgkong14@ciomp.ac.cn*

[b]*University of Chinese Academy of Sciences, Beijing 100049, China*

[c]*Van't Hoff Institute for Molecular Sciences, University of Amsterdam, 1098 XH Amsterdam, The Netherlands. E-mail: h.zhang@uva.nl*

† Electronic supplementary information (ESI) available: Fitted curves of the decay profiles of the $^1D_2 \rightarrow {}^3F_4$ transition and $^1G_4 \rightarrow {}^3H_6$ transition. See DOI: 10.1039/c3nr01916k

2 Experimental section

2.1 Synthesis of β-$NaYF_4$:Yb^{3+}, Tm^{3+} nanoparticles

β-$NaYF_4$ was prepared following a reported procedure with some modifications.[19] Specifically, 1 mmol of the lanthanide chlorides (0.795 mmol $YCl_3 \cdot 6H_2O$, 0.20 mmol $YbCl_3 \cdot 6H_2O$ and 0.005 mmol $TmCl_3 \cdot 6H_2O$) were taken in a 100 ml 3-necked flask, where 15 ml of octadecene and 6 ml of oleic acid were also added. The flask was then heated to 160 °C under an argon atmosphere and held at this temperature for 30 min to achieve a homogenous solution. Subsequently, the flask was cooled to room temperature and 10 ml methanol solution containing 4 mmol NH_4F and 2.5 mmol NaOH and $LiOH \cdot H_2O$ was added dropwise. The resulting solution was stirred at room temperature and heated slowly to 70 °C for 30 min until the methanol had evaporated. The reaction vessel was then brought under a gentle flow of argon and heated up to 300 °C and held at that temperature for 90 min. The flask was then cooled to room temperature and the nanoparticles were precipitated by adding ethanol, centrifuged and washed with ethanol. The isolated oleate-stabilized nanoparticles were stored as a 1 wt% dispersion in 6 ml of cyclohexane.

2.2 Characterization

XRD studies were performed on powders using a Bruker D8 Focus X-ray diffractometer system with monochromatized Cu-Kα radiation (λ = 1.5418 Å). Upconversion emission spectra were acquired using a Jobin Yvon LabRam Raman spectrometer system equipped with holographic gratings of 1800 and 600 grooves per mm resolution, respectively, and a Peltier air-cooled CCD detector. A 980 nm laser diode was used as the excitation source and the beam was focused (about 8 cm focal length) to a spot size of approximately 0.2 mm in diameter to reach high excitation density. Upconversion luminescence kinetics was recorded with a 500 MHz Tektronix digital oscilloscope and the excitation was realized by a nanosecond pulse train at 980 nm from an optical parametric oscillator. Precise control of the sample temperature (0.1 °C) was achieved by means of a Linkam THMS600 temperature-programmable heating/cooling microscope stage. The THMS stage was used in conjunction with a Linkam LNP cooling system when cooling. In the excitation power-dependent upconversion luminescence experiments, the power density increased step by step to guarantee that the thermal equilibrium was reached, and the collection time was about 30 s.

3 Results and discussion

The crystal structures and the phase purity of the as-prepared products were examined by XRD. The typical XRD patterns of them the as-prepared products are presented in Fig. 1. All diffraction peaks of the samples matched very well with the 100, 110, 101, 200, 111, 201, 210, 002, 300, 211, 102, 112, 220, 202, and 310 reflection peaks of hexagonal $NaYF_4$ (JCPDS 16-0344). No other impurity peaks were detected, which revealed that pure β-$NaYF_4$ had been fabricated. Interestingly, when zooming in on the pattern, the positions of the diffraction peaks were found to shift slightly with the Li^+ doping concentration. An example is given in Fig. 2, where the main diffraction peak at 17.1° is shifted towards a larger angle as the Li^+ ion concentration is increased up to 7 mol%, then moved backwards when the Li^+ ion concentration continued to increase to 15 mol%. A similar behaviour was also observed for the other peaks. It is known that a larger lattice constant is related to a smaller diffraction angle, and *vice versa*.[20] Therefore, the structure of the

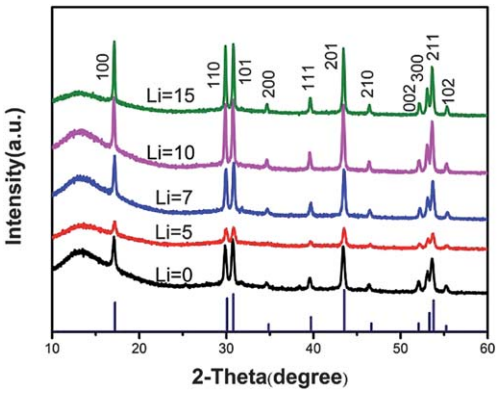

Fig. 1 X-ray diffraction patterns of $NaYF_4$:Yb^{3+}, Tm^{3+} nanocrystals doped with Li^+ ions (0, 5, 7, 10, 15 mol%) in doping concentration, contrasted with the standard pattern of JCPDS no. 16-0334.

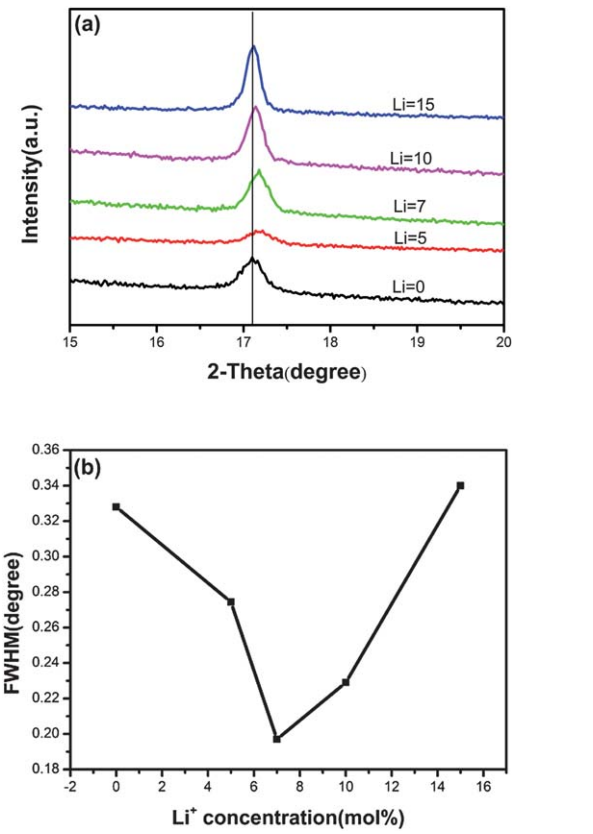

Fig. 2 (a) The main diffraction peaks of the $NaYF_4$:Yb^{3+}, Tm^{3+} nanocrystals with different concentrations of Li^+ ions; (b) FWHM of 17.1° peak *vs.* concentrations of Li^+ ions.

lattice of the $NaYF_4$ corresponded non-monotonously to the Li^+ ion concentration: at low doping concentrations the crystal lattice is shrinking, but at high concentrations the lattice is expanding. As far as the doping method of the Li^+ ions is concerned, this non-monotonous behaviour should correspond to the substitution and interstitial sites of the Li^+ ions, which can be determined using Bragg's law $2d\sin\theta = n\lambda$, where d is the interplanar distance, θ is the diffraction angle, and λ is the diffraction wavelength. When Li^+ ions substitute Na^+ ions the lattice shrinks, as the interplanar distance is reduced, resulting in the θ becoming larger; when Li^+ ions were at interstitial sites, the interplanar distance increased and θ became smaller. The effective ionic radius of Na^+ and Li^+ are 0.97 Å and 0.68 Å, respectively.[16] So Li^+ ions are small enough to substitute Na^+ or to occupy interstitial sites. Similar results were also observed in the system of $NaGdF_4$:Yb^{3+}, Er^{3+} co-doped with Li^+ ions.[18]

Information on the size and crystallinity of the nanocrystals can be obtained from the width of the diffraction peaks. As shown in Fig. 2b, the full width at half maximum (FWHM) was gradually narrowed as the Li^+ ion concentration increased up to 7 mol%, and then broadened as the concentration further increased. Combining these results with the morphology information shown in Fig. 3, where Li^+ ion-doping caused little change in the size and shape, leads to the conclusion that the crystallinity of the nanoparticles was improved when the Li^+ ion concentration was lower than 7 mol%, and reduced when the Li^+ ion concentration was greater than 7 mol%. It is worth mentioning that both the substitution of Na^+ ions and the occupation of interstitial sites can tailor the local crystal field around the Tm^{3+} ions, which is expected to affect its upconversion luminescence intensity.

The average crystalline sizes can be estimated from Scherrer's equation:

$$D = \frac{0.89\lambda}{\beta\cos\theta}$$

where D represents the crystallite size, λ stands for the wavelength of the X-ray, β is the corrected half width of the diffraction peak, and θ denotes the diffraction angle. The factor 0.89 is characteristic of a spherical particle.

The sizes of the $NaYF_4$:Yb^{3+}, Tm^{3+} nanocrystals doped with Li^+ concentrations of 0, 5, 7, 10 and 15% were calculated to be about 45, 48, 53, 50 and 46 nm, respectively. To confirm the result, the TEM images of the $NaYF_4$:Yb^{3+}, Tm^{3+} nanocrystals co-doped with different concentrations of Li^+ ions are given in Fig. 3. The diameters of the nanoparticles in Fig. 3 were about 50 nm, which are consistent with results drawn from the X-ray diffraction (XRD) study. Thus, the introduction of Li^+ ions resulted in only a little change in the size of the $NaYF_4$ nanocrystals. The HRTEM image (Fig. 3f) of a $NaYF_4$ nanoparticle with a doping of 7 mol% Li^+ ions shows distinct lattice fringes with a d-spacing of 0.37 nm, ascribed to the (110) plane, which shows that the NPs have a single crystalline feature.

Fig. 4 shows the UC luminescence spectra of $NaYF_4$:Yb^{3+}, Tm^{3+} nanocrystals doped with different concentrations of Li^+ ions at room temperature under 980 nm laser excitation. Four distinct peaks in the range of 300–700 nm were observed. The dominant violet and blue emissions at 450 nm and 479 nm were assigned to the $^1D_2 \rightarrow {}^3F_4$ and $^1G_4 \rightarrow {}^3H_6$ transitions, respectively, the red emission at 646 nm was attributed to the $^1G_4 \rightarrow {}^3F_4$ transition, and the ultraviolet emission at 360 nm was attributed to the $^1D_2 \rightarrow {}^3H_6$ transition. In addition, the violet and blue UC luminescence were distinctly enhanced when the concentration of the Li^+ ions changed from 5 to 7 mol%, while the enhancing magnitude differed for the red emissions. The strongest UC emission was observed in the sample with a Li^+ concentration of 7 mol% and the violet and blue emissions were about 8 and 5 times stronger than the Li^+-free sample. The somewhat mild enhancement of the UC emissions of $NaYF_4$:Yb^{3+}, Tm^{3+} nanocrystals by Li^+ ions compared with the report of the $NaGdF_4$:Yb^{3+}, Er^{3+} nanocrystals could have something to do with to the matching of the energy levels between Tm^{3+} and Yb^{3+} being not as good as that between Er^{3+} and Yb^{3+}.

The inset of Fig. 4 shows the Li^+ concentration dependence of the integral intensity of 452 nm and 479 nm. The similar trend suggests that they have the same UC pathway. As shown in the inset of Fig. 4, the violet and blue UC emissions were enhanced dramatically with the increase of Li^+ ion concentration. When the Li^+ ion concentration reached 7 mol%, the UC luminescence

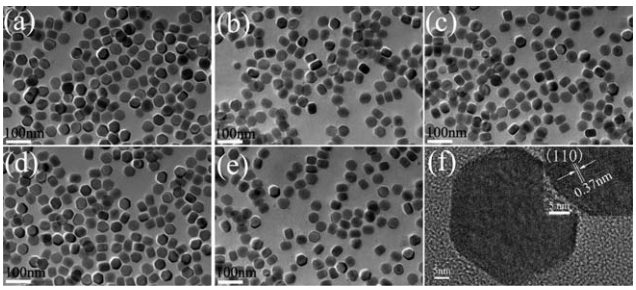

Fig. 3 TEM images of $NaYF_4$:Yb^{3+}, Tm^{3+} nanocrystals doped with different concentrations of Li^+ ions: (a) 0 mol% Li^+, (b) 5 mol% Li^+, (c) 7 mol% Li^+, (d) 10 mol% Li^+, (e) 15 mol% Li^+, (f) HRTEM image of nanoparticle doping with 7 mol% Li^+ (the inset is the zoomed part of the HRTEM image).

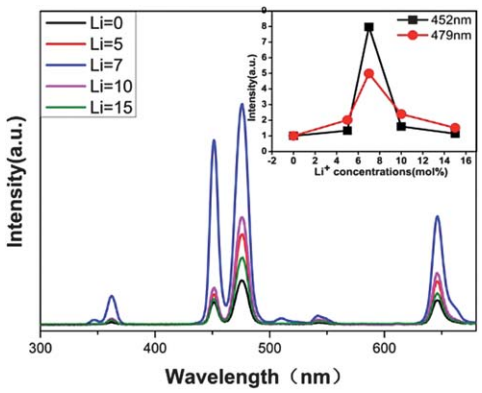

Fig. 4 UC luminescence spectra of $NaYF_4$:Yb^{3+}, Tm^{3+} nanocrystals doped with different concentrations of Li^+ ions (0–15 mol%) under 980 nm excitation at room temperature (the concentration of Tm^{3+} was the same in all samples). The inset shows the integral intensity of the 452 nm and 479 nm emissions as a function of Li^+ ion concentration.

intensity reached its maximum, then the intensity was weakened with the further increase of Li^+ ion concentration, especially when the Li^+ ion concentration was over 10 mol%.

To visualize the improvement of the UC emission, the photographs of the upconversion luminescence of the $NaYF_4$:Yb^{3+}, Tm^{3+} nanocrystal solutions with different Li^+ ion concentrations in hexane (1 wt%) excited with a 980 nm laser diode (taken by a digital camera without any additional filter) are provided in Fig. 5. As shown in this figure, the fluorescent strength is significantly increased by introduction of Li^+ ions and the changes in fluorescence strength are clearly observed with the naked-eye. The luminescence intensity of the $NaYF_4$:Yb^{3+}, Tm^{3+} nanocrystals with 7 mol% Li^+ ions is the strongest, which was ascribed to the most asymmetric environment of Tm^{3+} in the sample, according to the results from Fig. 2.

In order to study the UC mechanism, the excitation power density dependencies of the UC luminescence were measured, as shown in Fig. 6. For the unsaturated upconversion process, the number of photons required to populate the upper emitting state can be described by the following relation:[21]

$$I_{up} \propto P^n$$

where I_{up} is the upconversion emission intensity, P is the pump laser intensity, and n is the number of pump photons required. As shown in Fig. 6, the slopes (n values) obtained were 3.22 and 2.57 for the 452 and 479 nm emissions in the $NaYF_4$:Yb^{3+}, Tm^{3+} sample when introducing 7 mol% Li^+, which are slightly smaller than the n values (3.77 and 2.76 for 452 and 479 nm, respectively) for the $NaYF_4$:Yb^{3+}, Tm^{3+} nanocrystals (Fig. 6a), indicating that the violet and blue emissions are four- and three-photon processes for the samples with and without Li^+ ions. The same behavior was observed in other samples (see the ESI, Fig. S1†). The Li^+ ions cannot absorb 980 nm photons and cannot transfer its energy to Tm^{3+}, which indicates that the mechanisms for UC radiation have not been affected by the introduction of Li^+ ions. However, the n values change slightly with the change of Li^+ ion concentration and are smaller than that of the $NaYF_4$:Yb^{3+}, Tm^{3+} nanocrystals without Li^+ ions. It was reported that a realistic upconversion system that produces detectable upconversion luminescence will

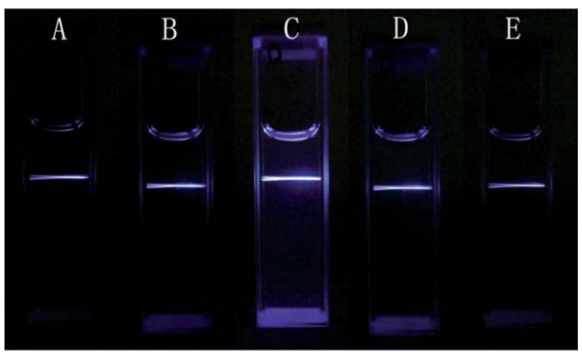

Fig. 5 Photographs of the upconversion luminescence of the $NaYF_4$:Yb^{3+}, Tm^{3+} nanocrystals in hexane: (A) 0 mol% Li^+, (B) 5 mol% Li^+, (C)7 mol% Li^+, (D) 10 mol% Li^+, (E) 15 mol% Li^+, taken with a digital camera without any additional filter under the excitation of a 980 nm laser diode.

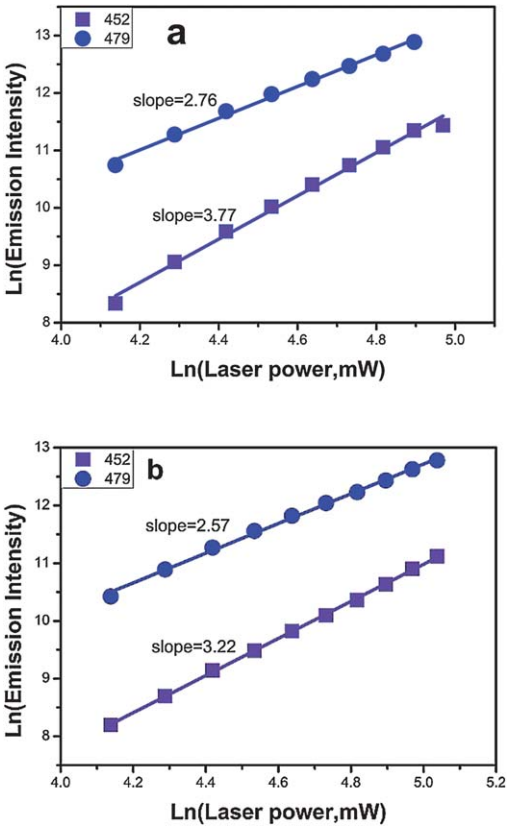

Fig. 6 Pump power dependence of the violet and blue emission of $NaYF_4$:Yb^{3+}, Tm^{3+} nanocrystals: (a) 0 mol% Li^+, (b) 7 mol% Li^+.

exhibit an intensity-*versus*-power dependence, which is less than the assumed P^n. Competition between the upconversion process and linear decay by luminescence to the ground state or relaxation into the next lower-lying state for the depletion of the intermediate excited states result in a significantly reduced slope.[22] A larger upconversion rate means a smaller slope. Introducing Li^+ ions can increase the upconversion transition rate leading to the enhancement of upconversion luminescence.

Moreover, we measured the time behaviour of the $^1D_2 \rightarrow {}^3F_4$ (452 nm) and $^1G_4 \rightarrow {}^3H_6$ (479 nm) transitions for the $NaYF_4$:Yb^{3+}, Tm^{3+} nanocrystals with 0–15 mol% Li^+ ions. Fig. 7 shows the normalized decay profiles of the $^1D_2 \rightarrow {}^3F_4$ transition at 452 nm and $^1G_4 \rightarrow {}^3H_6$ transition at 479 nm in the samples. All the decay curves of the samples could be well fitted to a double exponential function (see ESI, Fig. S2 and S3†):[23]

$$I(t) = I_0 - A_1\exp(-t/\tau_1) + A_2\exp(-t/\tau_2)$$

where I and I_0 are the luminescence intensities at time t and 0. A_1 and A_2 are constants, t is time, τ_1 and τ_2 represent the rise and decay times of the transient for the exponential components.

When analyzing the curves, one has to realize that the luminescence decay does not always represent the depopulation of the emissive state, and a luminescence rise does not always represent the population of the emissive state as well. This is due to the fact that when a rise and decay component coexist in the luminescence kinetics, the decay is always the longer one,

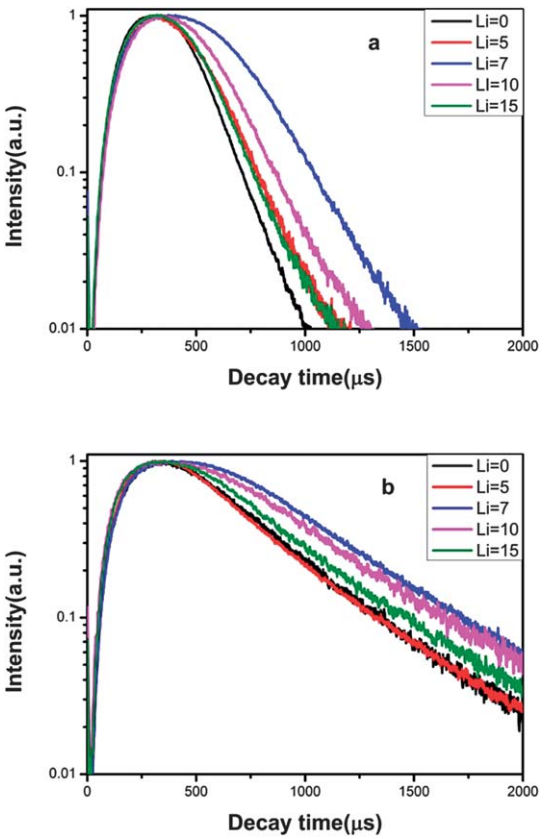

Fig. 7 Decay profiles of $^1D_2 \rightarrow {}^3F_4$ transition (a) and $^1G_4 \rightarrow {}^3H_6$ transition (b) under 980 nm excitation.

even if the population is slower than the depopulation. Upconversion luminescence of rare earth ions is just one of such examples. Because the intermediate states mediate the upconversion process, for example $^3H_4$ and $^3F_4$ have much longer lifetimes relative to the final upconversion emission states, and for example the $^1D_2$ and $^1G_4$ states, the rise components in our measurements are determined by the lifetimes of the latter states, whereas the intermediate states, that is $^3H_4$ and $^3F_4$ states, determine the decay components of the upconversion luminescence kinetics. Therefore, τ_1 mainly reflects the nature of the $^1D_2$ and $^1G_4$ states, and τ_2 represents the lifetime of the $^3H_4$ and $^3F_4$ states. The fitted lifetimes of the $^1D_2$ and $^1G_4$ states of the Tm^{3+} ions for the $NaYF_4$:Yb^{3+}, Tm^{3+} nanocrystals with 0–15 mol% Li^+ ions are listed in Table 1.

All the decay lifetimes of the $^1D_2$ state and $^1G_4$ state of $NaYF_4$:Yb^{3+}, Tm^{3+}, with different concentrations of Li^+ ions, were longer than that of the $NaYF_4$:Yb^{3+}, Tm^{3+} nanocrystals without Li^+ ions, indicating that the doping of Li^+ does improve the luminescence. Furthermore, the lifetimes τ_1 and τ_2 of the $^1D_2$ and $^1G_4$ states in the sample with 7 mol% Li^+ ions were the longest among the samples, illustrating that at this doping concentration, the lifetime of the intermediate states τ_2 was the longest, which facilitates the population of the emission state, resulting in the longest lifetime of τ_1.

From the steady-state and dynamic upconversion spectroscopy analysis we can visualize the internal structure evolution of

Table 1 Lifetimes of the $^1D_2$ and $^1G_4$ states of Tm^{3+} ions in the $NaYF_4$:Yb^{3+}, Tm^{3+} nanocrystals with 0–15 mol% Li^+ ions

Li^+ concentration (mol%)	$^1D_2$		$^1G_4$	
	τ_1/μs	τ_2/μs	τ_1/μs	τ_2/μs
0	192	256	224	305
5	261	283	233	310
7	264	378	304	432
10	188	308	262	380
15	173	298	229	310

the $NaYF_4$ nanocrystals when Li^+ ions are added increasingly. At beginning, with a low Li^+ concentration, Na^+ is replaced and in this period the shrinking of the lattice results in lattice perfection and the UC emission is consequently enhanced, until a concentration of 7 mol% Li^+ is reached, when most of the Na^+ ions are substituted. Continuously adding Li^+ into the crystal causes more and more Li^+ ions to occupy interstitial sites, which will cause defect centers and the UC emission is thus reduced.

Fig. 8 shows the possible upconversion luminescence mechanism diagram of the $NaYF_4$:Yb^{3+}, Tm^{3+}. One energy transfer step from the Yb^{3+} ion to Tm^{3+} ion populates the $^3H_5$ level of Tm^{3+} from $^3H_6$. The $^3H_5$ decays rapidly to the $^3F_4$ level. The second energy transfer step raises the Tm^{3+} ion from $^3F_4$ to $^3F_2$, which quickly decays to $^3H_4$. Subsequently, the third transfer step raises the Tm^{3+} ion from $^3H_4$ to $^1G_4$, which can yield a blue emission upon radiative relaxation back to $^3H_6$. A fourth energy transfer step from the Yb^{3+} ion to Tm^{3+} ion may also take place to populate the Tm^{3+} ion from the $^1G_4$ level to $^1D_2$, which is, however, usually less efficient due to the relatively large energy mismatch. It is well known that the electronic transitions of rare earth ions between different energy levels come from a $4f^N$ configuration. According to the selection rule: $|\Delta J| = 2$, $|\Delta L| = 0, \pm 1$ and $\Delta S = 0$, the electric dipole transitions are forbidden in the same parity state. However, this prohibition could be broken if the crystal field is changed and the inversion symmetry is relieved, which results in the increasing of the electric dipole transitions probability.

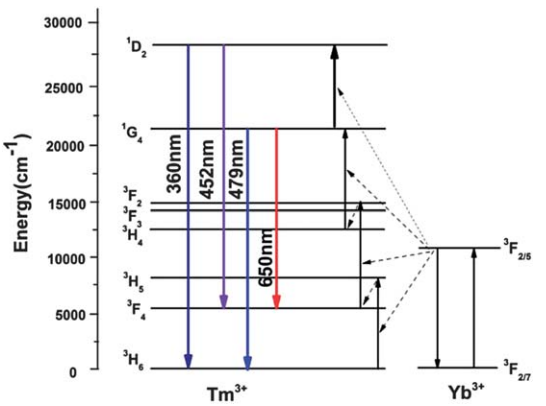

Fig. 8 Schematic illustration of the energy levels involved in the upconversion process of Tm^{3+} with Yb^{3+} as the promoter for $NaYF_4$:Yb^{3+}, Tm^{3+} NCs.

Therefore, in the case of the upconversion scenario, a less symmetric crystal symmetry is generally favorable for higher UC efficiency, since intermixing of the lanthanide ion's f states with higher electronic configurations can be more pronounced.[24,25]

The crystal structure of $NaYF_4$ is hexagonal with the *P*63*m* space group. The primitive unit cell of $NaYF_4$ has three cationic sites, one for rare earth ions, one for both rare earth and sodium ions, and the third for sodium ions. With the introduction of Li^+ ions, the Li^+ ions are substitutional or interstitial in behavior or coexist in the two ways; either way would change the surrounding environment of Tm^{3+} ions and the crystal field. At the same time, introducing Li^+ ions could lead to a change in the electron distribution density. The change in the environment of the rare earth could lead to hypersensitive electron transition.[26] Both types of Li^+ occupancies lower the local crystal field symmetry around the Tm^{3+} and Yb^{3+} ions, which is in favor of breaking the forbidden transition of the rare earth ions so that the luminescence intensity of Tm^{3+} was enhanced.

4 Conclusions

In conclusion, β-$NaYF_4$:Yb^{3+}, Tm^{3+} nanocrystals doped with different concentrations of Li^+ ions were first synthesized in search of a novel approach of enhancing UC luminescence. The significant enhancement of the UC emission in $NaYF_4$:Yb^{3+}, Tm^{3+} nanocrystals as a result of the introduction of Li^+ ions without changes in phase and morphology were observed. In contrast to the lithium-free $NaYF_4$:Yb^{3+}, Tm^{3+}, the UC emission intensities of 452 nm and 479 nm of the NPs co-doped with 7 mol% Li^+ ions were increased by about 8 and 5 times, respectively. The mechanisms for the enhancement of the upconversion emission were also discussed, which can be attributed to the improvement of the crystallinity and the reduced local crystal field symmetry around the Tm^{3+} ions. This work facilitates the use of a Li^+ doping strategy to enhance the luminescence intensity of lanthanide-doped nanoparticles.

Acknowledgements

This work was financially supported by the NSF of China (11004189, 11174277, 10904142, 61275202 and 61275197), a joint research program between the CAS of China and KNAW of the Netherlands, the IOP program of the Netherlands, and the John van Genus foundation.

Notes and references

1 T. R. Hinkliin, S. C. Rand and R. M. Laine, *Adv. Mater.*, 2008, **20**, 1270.
2 X. Wang, X. G. Kong, Y. Yu, Y. J. Sun and H. Zhang, *J. Phys. Chem. C*, 2007, **111**, 1511.
3 (*a*) J. Zhang, W. S. Wang, L. Q. An, M. Liu and L. D. Chen, *J. Lumin.*, 2006, **8**, 122; (*b*) J. Limpert, F. Stutzki, F. Jansen, H. Otto, T. Eidam, C. Jauregui and A. Tünnermann, *Light: Sci. Appl.*, 2012, **1**, 8.
4 (*a*) S. F. Lim, R. Riehn, W. S. Ryu, N. Khanarian, C. K. Tung, D. Tank and R. H. Austin, *Nano Lett.*, 2006, **6**, 169; (*b*) G. Y. Chen, Y. G. Zhang, G. Somesfalean, Z. G. Zhang, Q. Sun and F. P. Wang, *Appl. Phys. Lett.*, 2006, **89**, 163105.
5 L. Y. Wang and Y. D. Li, *Chem. Commun.*, 2006, 2557.
6 R. Kumar, M. Nyk, T. Y. Ohulchanskyy, C. A. Flask and P. N. Prasad, *Adv. Funct. Mater.*, 2009, **19**, 853.
7 M. Wang, C. Mi, Y. Zhang, J. Liu, F. Li, C. Mao and S. Xu, *J. Phys. Chem. C*, 2009, **113**, 19021.
8 P. Zhang, W. Steelant, M. Kumar and M. Scholfield, *J. Am. Chem. Soc.*, 2007, **129**, 4526.
9 (*a*) W. B. Niu, S. L. Wu, S. F. Zhang and L. Li, *Chem. Commun.*, 2010, **46**, 3908; (*b*) S. Liang, Y. Liu, Y. Tang, Y. Xie, H. Z. Sun, H. Zhang and B. Yang, *J. Nanomater.*, 2011, **2011**, 302364; (*c*) F. Wang, Y. Han, C. S. Lim, Y. H. Lu, J. Wang, J. Xu, H. Y. Chen, C. Zhang, M. H. Hong and X. G. Liu, *Nature*, 2010, **463**, 1061; (*d*) D. Q. Chen, Y. L. Yu, F. Huang, P. Huang, A. P. Yang and Y. S. Wang, *J. Am. Chem. Soc.*, 2010, **132**, 9976; (*e*) F. Wang, J. A. Wang and X. G. Liu, *Angew. Chem., Int. Ed.*, 2010, **49**, 7456.
10 G. S. Yi and G. M. Chow, *Adv. Funct. Mater.*, 2006, **16**, 2324.
11 D. Li, B. A. Dong, X. Bai, Y. Wang and H. W. Song, *J. Phys. Chem. C*, 2010, **114**, 8219.
12 (*a*) F. Vetrone, R. Naccache, V. Mahalingam, C. G. Morgan and J. A. Capobianco, *Adv. Funct. Mater.*, 2009, **19**, 2924; (*b*) L. Sudheendra, V. Ortalan, S. Dey, N. D. Browning and I. M. Kennedy, *Chem. Mater.*, 2011, **23**, 2987.
13 (*a*) L. Sudheendra, V. Ortalan, S. Dey, N. D. Browning and I. M. Kennedy, *Chem. Mater.*, 2011, **23**, 2987; (*b*) N. Liu, W. P. Qin, G. S. Qin, T. Jiang and D. Zhao, *Chem. Commun.*, 2011, **47**, 7671; (*c*) W. Xu, S. Xu, Y. S. Zhu, T. Liu, X. Bai, B. Dong, L. Xu and H. W. Song, *Nanoscale*, 2012, **4**, 6971.
14 X. J. Xue, F. Wang and X. G. Liu, *J. Mater. Chem.*, 2011, **21**, 13107.
15 Q. M. Huang, J. C. Yu, E. Ma and K. M. Lin, *J. Phys. Chem. C*, 2010, **114**, 4719.
16 N. Dhananjaya, H. Nagabhushana, B. M. Nagabhushana, B. Rudraswamy, C. Shivakumara and R. Chakradhar, *J. Alloys Compd.*, 2011, **509**, 2368.
17 G. Y. Chen, H. C. Liu, H. J. Liang, G. Somesfalean and Z. G. Zhang, *J. Phys. Chem. C*, 2008, **112**, 12030.
18 Q. Cheng, J. h. Sui and W. Cai, *Nanoscale*, 2012, **4**, 779–784.
19 Z. Q. Li and Y. Zhang, *Nanotechnology*, 2008, **19**, 345606.
20 X. Q. Chen, Z. K. Liu, Q. Sun, M. Ye and F. P. Wang, *Opt. Commun.*, 2011, **284**, 2046.
21 M. Z. Yang, Y. Sui, S. P. Wang, X. J. Wang, Y. Q. Sheng, Z. G. Zhang, T. Q. Lu and W. F. Liu, *Chem. Phys. Lett.*, 2010, **492**, 40.
22 M. Pollnau, D. R. Gamelin, S. R. Lüthi, H. U. Güdel and M. P. Hehlen, *Phys. Rev. B: Condens. Matter Mater. Phys.*, 2000, **61**, 3337.
23 J. Y. Sun, W. H. Zhang, H. Y. Du and Z. P. Yang, *Infrared Phys. Technol.*, 2010, **53**, 388.
24 B. R. Judd, *Phys. Rev.*, 1962, **127**, 750.
25 G. S. Ofelt, *J. Chem. Phys.*, 1962, **37**, 511.
26 T. Huang and W. Hsieh, *J. Fluoresc.*, 2009, **19**, 511.